European Journal of Pharmaceutics and Biopharmaceutics 72 (2009) 397–404

Contents lists available at ScienceDirect

European Journal of Pharmaceutics and Biopharmaceutics

journal homepage: www.elsevier.com/locate/ejpb

Research paper

# A high relaxivity Gd(III)DOTA-DSPE-based liposomal contrast agent for magnetic resonance imaging

Sjoerd Hak [a], Honorius M.H.F. Sanders [a,b], Prashant Agrawal [a], Sander Langereis [c], Holger Grüll [a,c], Henk M. Keizer [d], Francesca Arena [e], Enzo Terreno [e], Gustav J. Strijkers [a], Klaas Nicolay [a,*]

[a] Department of Biomedical Engineering, Eindhoven University of Technology, Eindhoven, The Netherlands
[b] Department of Biomedical Engineering, Eindhoven University of Technology, The Netherlands
[c] Department of Bio-Molecular Engineering, Philips Research, High Tech Campus, Eindhoven, The Netherlands
[d] SyMO-Chem BV, Eindhoven, The Netherlands
[e] Department of Chemistry IFM and Molecular Imaging Center, University of Torino, Torino, Italy

ARTICLE INFO

*Article history:*
Received 16 May 2008
Accepted in revised form 30 September 2008
Available online 10 October 2008

*Keywords:*
Molecular imaging
Magnetic resonance imaging
Contrast agent
Liposomes
Gadolinium
Gd(III)DOTA-DSPE
Longitudinal relaxivity
cryo-TEM
Transmetallation

ABSTRACT

The field of molecular imaging aims to visualize and quantify (patho)physiological processes at the cellular and molecular level. Sensitive and site-targeted contrast agents are employed to visualize molecular constituents of processes of interest. The principal aim of this study was to develop a magnetic resonance imaging (MRI) detectable liposome with high relaxivity and stability. To this end, Gd(III)DOTA-DSPE was synthesized and incorporated in a liposomal formulation. The resulting liposomes were extensively characterized *in vitro* in terms of contrast agent efficiency and structural properties. The liposomes were shown to have a high longitudinal relaxivity, which is crucial for the detection of low concentration molecular markers in molecular imaging studies. We also demonstrated that Gd(III)DOTA-DSPE exhibits no detectable transmetallation upon incubation with Zn(II). This is important as it significantly contributes to the biocompatibility of the contrast agent. The present liposome preparation will serve as versatile and well characterized platform for molecular imaging and targeted drug delivery studies.



## 1. Introduction

In the last decade, a new field of research in medical imaging has emerged, referred to as 'molecular imaging', which aims to visualize and quantify (patho)physiological processes at the cellular and molecular level [1]. As molecular markers of physiological processes are too small and often present in concentrations too low to be directly detected using conventional imaging approaches, sensitive site-targeted contrast agents are employed in combination with a non-invasive imaging modality, such as magnetic resonance imaging (MRI). The recent applications include the development of nanocarriers for combined imaging and drug delivery. Hence, MRI detectable nanoparticles endowed with specific targeting capabilities are designed to report on the localization of specific biomarkers as well as on the drug release process and therapeutic outcome [2].

Signal intensities in MR images of living tissues depend on the so-called longitudinal and transverse relaxation times ($T_1$ and $T_2$) of protons in primarily water and lipids. The majority of MR contrast agents act by shortening the relaxation times of water protons. The efficiency by which a contrast agent shortens the $T_1$ is called the longitudinal relaxivity, $r_1$ (units, $mM^{-1}s^{-1}$). The relation between the longitudinal relaxation rate ($1/T_1$) of the bulk water protons and the $T_1$-relaxivity of a contrast agent is described by

$$\frac{1}{T_1} = \frac{1}{T_{1,\text{tissue}}} + r_1[\text{CA}], \tag{1}$$

where $T_1$ and $T_{1,\text{tissue}}$ are the longitudinal relaxation times in the presence and in the absence of the MR contrast agent, respectively, and [CA] is the concentration of the contrast agent. The same equation holds for the transversal relaxation time and relaxivity, $T_2$ and $r_2$, respectively. Most MRI contrast agents are based either on iron-oxide particles or on Gd(III) complexes. Iron-oxide-based contrast agents generally have a high $r_2/r_1$ ratio and are therefore suitable to generate negative contrast (dark areas) in $T_2$-weighted images, while Gd(III)-based contrast agents have a relatively low $r_2/r_1$ ratio, and are most frequently employed to generate positive contrast (bright spots) in $T_1$-weighted images.

The sensitivity of MRI for detecting low concentrations of contrast agents is relatively low, and is often not sufficient to visualize

* Corresponding author. Biomedical NMR, Department of Biomedical Engineering, Eindhoven University of Technology, P.O. Box 513, Eindhoven 5600, The Netherlands.
*E-mail address:* k.nicolay@tue.nl (K. Nicolay).

0939-6411/$ - see front matter © 2008 Elsevier B.V. All rights reserved.
doi:10.1016/j.ejpb.2008.09.017

sparse molecular epitopes. This problem can be overcome by using contrast agents with a very high relaxivity or by using nanoparticles that contain a high payload of low-relaxivity contrast agents. In case of Gd(III) contrast agents, nanoparticles based on colloidal lipid systems such as liposomes and micelles are very suitable as they can be equipped with hundreds to ten-thousands of Gd(III) complexes [3]. Micelles and liposomes have been studied extensively in the past decades as drug carrier systems [4,5]. More recently, these particles have also been employed successfully as MRI contrast agents to do cell labeling [6] and to visualize, for example, markers of tumor angiogenesis [7], the pathophysiology of atherosclerotic plaques [8,9], autoimmune encephalitis [10] and apoptosis [11].

The principal aim of this study was to develop a lipid-based MRI detectable liposome with improved relaxivity and stability compared to previously published formulations [12,3], and to provide an extensive characterization in terms of MRI and structural properties. The presented liposome preparation contains a high payload of a novel paramagnetic lipid molecule, Gd(III)DOTA-DSPE. Next to the synthesis of this compound and the liposome preparation procedure, the characterization of the liposomes is described.

## 2. Materials and methods

### 2.1. Materials

1,2-Distearoyl-*sn*-glycero-3-phosphocholine (DSPC), 1,2-distearoyl-*sn*-Glycero-3-phosphoethanolamine-*N*-[methoxy(polyethyleneglycol)-2000] (PEG2000-DSPE), and cholesterol (Chol) were purchased from Avanti Polar Lipds (Albaster, AL). Gd(III)DTPA-bis(sterylamide) (Gd(III)DTPA-BSA) was obtained from Gateway Chemical Technology (St. Louis, MO). Gd(III)DTPA (Magnevist®) was obtained from Schering (Berlin, Germany). Gd(III)-HPDO3A (Prohance®) was purchased from Bracco Diagnostics (Milan, Italy). 1,2-Distearoyl-*sn*-glycero-3-phosphoethanolamine (DSPE) was purchased from Alexis Biochemicals (Lausen, Switzerland). Dichloromethane (DCM) was dried over $P_2O_5$. Dimethylformamide (DMF) was dried over molsieves. Unless stated otherwise, all other reagents and chemicals were obtained from commercial sources and used without further purification. All hygroscopic compounds were stored in a desiccator over $P_2O_5$. *N*,*N*′-Diisopropylethylamine (D*i*PEA) was stored over KOH pellets.

### 2.2. Instrumentation

$^1$H NMR, $^{13}$C NMR and $^{31}$P NMR spectra were recorded on a Gemini-2000 300 MHz spectrometer from Varian (Palo Alto, CA), a Varian Mercury V× 400 MHz spectrometer or a Varian Unity Inova 500 MHz spectrometer at 25 °C. Chemical shifts are given in ppm ($\delta$) values. Infrared spectra were recorded on a Perkin–Elmer (Waltham, Massachusetts) 1605 FT-IR spectrometer. MALDI-TOF spectra were obtained on a Perspective Biosystems Voyager DE-Pro (Hertford, UK). The HPLC system was coupled to an evaporative light scattering detector (ELSD), Alltech ELSD 2000 (Nicholasville, UK). All HPLC runs were executed with a 0.5 mL/min flow rate using a Kromasil (Bohus, Sweden) C18 column (150 × 3.2 mm).

### 2.3. Synthesis

A schematic of the synthesis showing the organic structures of the building blocks and intermediates can be found in Fig. 1. The numbering of the structures in Fig. 1 corresponds to the numbering of the structures in the text.

### 2.4. DOTA-based building block (3)

Tris-*t*-butyl DOTA (**3**) intermediate was synthesized according to the literature procedure [13,14]. In this procedure first the tris-*t*-butyl-ester of cyclen was formed, followed by alkylation with benzyl bromoacetate and hydrogenation.

### 2.5. Tris-t-Bu-DOTA-DSPE (4)

DOTA-based building block **3** (1.50 g, 2.62 mmol) was added to a solution of HSTU (0.990 g, 0.276 mmol) and DiPEA (1.60 mL, 9.52 mmol) in dry DMF (10 mL). The mixture was stirred for 1 h at room temperature under an argon atmosphere. To the obtained yellowish solution, a solution of DSPE (**2**) (0.178 g, 2.38 mmol) in $CHCl_3$ (15 mL) was added under an argon atmosphere. The temperature was increased to 45 °C, and after approximately 10 min a clear solution was obtained. This solution was stirred for another 2 h at 45 °C. After cooling, the solution was stirred overnight at room temperature. The solution was concentrated under reduced pressure, co-evaporated with toluene (2 × 20 mL) and $CHCl_3$ (2 × 20 mL). The product was precipitated in 1:1 *v*/*v* water/MeOH. The yellowish precipitate was isolated by means of centrifugation. The resulting pellet was dissolved in $CHCl_3$, and concentrated *in vacuo*. The resulting solid was redissolved in 50 mL diethyl ether (some heating was needed), and washed with demi water (20 mL). Subsequently, the organic phase was concentrated *in vacuo*, resulting in **4** (2.93 g, 2.25 mmol) as a yellowish solid in 95% yield. $^1$H NMR ($CDCl_3$): $\delta$ = 9.6 (br t, 1H, NH), 5.2 (m, 1H, H2), 4.5–4.4 (m, 1H, $J_1$ = 12.0 Hz, $J_2$ = 3.4 Hz, H1), 4.3–4.2 (m, 1H, $J_1$ = 12 Hz, $J_2$ = 6.4 Hz, H1′), 4.1–3.9 (m, 4H, H3{2H} + $POCH_2CH_2NHCO${2H}), 3.6–2.0 (br m, 26 H, $NCH_2CH_2N$ {16H} + $NCH_2CO$ {8H} + $POCH_2CH_2NHCO$ {2H}), 2.3–2.2 (m, 4H, $CH_3(CH_2)_{15}CH_2CO$),1.7–1.0 (m, 87H), 0.9 (t, 6H, $J$ = 6.8 Hz, $CH_2CH_3$). The assignment of the $^1$H NMR spectrum is confirmed by $^1$H,$^1$H COSY. $^{13}$C NMR ($CDCl_3$, 125 MHz): $\delta$ = 173.5 (C═O), 173.1 (C═O), 173.0 (C═O), 170.9 (C═O), 81.9 ($C(CH_3)_3$), 70.8–70.7, 63.3–63.0 (multiple signals), 56.4, 55.7, 54–47 (set of two broad signals), 41.9, 34.4, 34.2, 31.9, 29.7–29.0 (multiple signals), 27.9, 24.9, 22.7, 14.1. $^{31}$P NMR ($CDCl_3$): $\delta$ = 1.4. FT-IR (ATR): $\nu$ ($cm^{-1}$) 3212 (NH stretch), 2924, 2853, 1729, 1668, 1567, 1456, 1381, 1369, 1312, 1227, 1163, 1066 and 908. MALDI-TOF (positive mode): *m*/*z* $[C_{69}H_{132}N_5O_{15}P_1 + H]^+$ Calcd. 1302.9 Da.; Obsd. 1302.8 Da.; $[M + Na]^+$ Calcd. 1324.9 Da.; Obsd. 1324.8 Da. MALDI-TOF (negative mode): *m*/*z* $[M - H]^-$ Calcd. 1300.9 Da.; Obsd. 1300.7 Da.

### 2.6. DOTA-DSPE (5)

TFA (5 mL) was added to a solution of **4** (2.93 g, 2.25 mmol) in $CHCl_3$ (15 mL) under an atmosphere of argon. The solution was vigorously stirred for 2 h at room temperature. The solution was concentrated under reduced pressure, redissolved in 1:3 *v*/*v* TFA/$CHCl_3$ (20 mL), and stirring was continued overnight at room temperature. The solution was concentrated under reduced pressure, and again dissolved in 1:3 *v*/*v* TFA/$CHCl_3$ (20 mL). The solution was vigorously stirred for 2 h at room temperature. Subsequently, the solution was concentrated under reduced pressure, co-evaporated with toluene (2 × 10 mL) and $CHCl_3$ (2 × 10 mL) and precipitated in $CH_3CN$ to yield **5** (0.309 g, 0.273 mmol) as a yellowish solid. $^1$H NMR spectroscopy confirmed the successful removal of the *tert*-butyl ester groups indicated by the absence of signals at 1.46 ppm. $^1$H NMR ($CDCl_3$): $\delta$ = 5.2 (br. m, 1H, H2), 4.4–2.4 (br. m, 32H), 2.3 (m, 4H, $CH_3(CH_2)_{15}CH_2CO$), 1.3–1.1 (m, 60H), 0.9 (t, 6H, $J$ = 6.4 Hz, $CH_2CH_3$).$^{31}$P NMR ($CDCl_3$): $\delta$ = −1.8. FT-IR (ATR): $\nu$ ($cm^{-1}$) 3356, 2918, 2851, 1728, 1675, 1467, 1387, 1163 and 1049. MALDI-TOF (positive mode): *m*/*z* $[C_{57}H_{108}N_5O_{15}P_1 + H]^+$

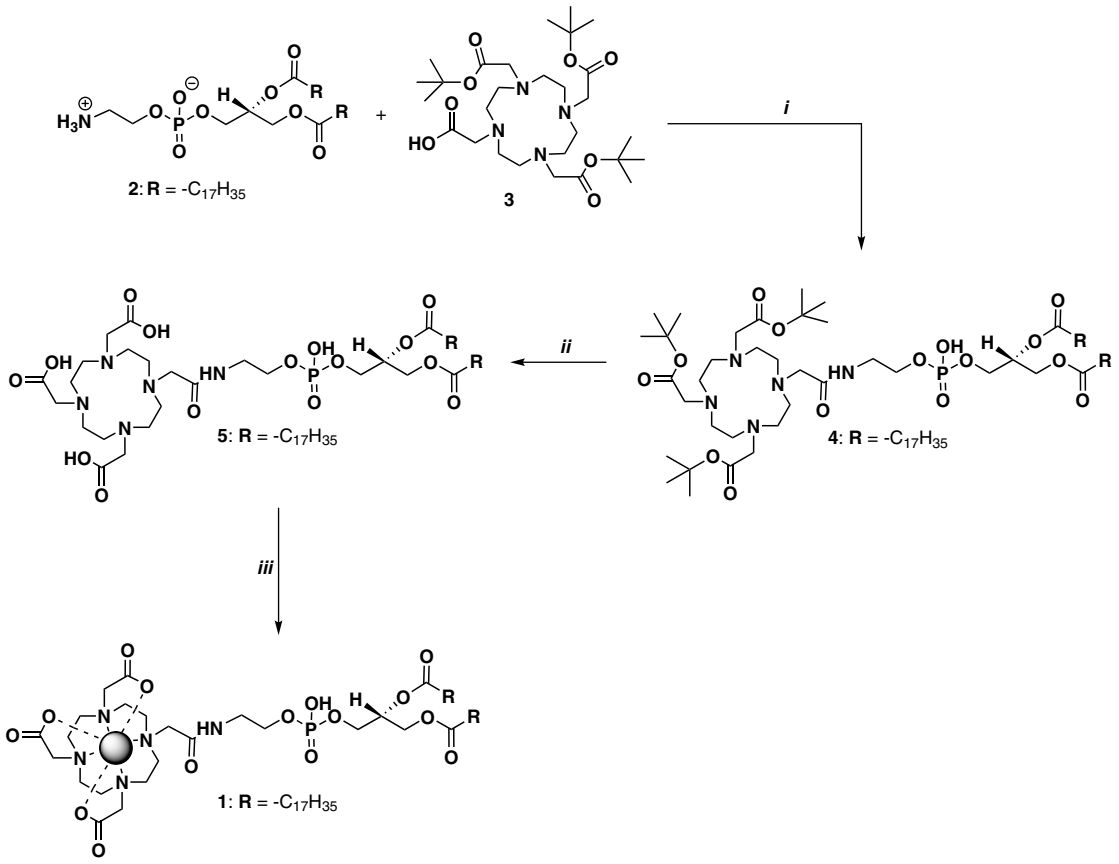


**Fig. 1.** Synthesis of Gd(III)DOTA-DSPE (1); (i) 1:1 *v*/*v* DMF/$CHCl_3$, HBTU, DiPEA; (ii) 1:2 *v*/*v* TFA/DCM; (iii) $Gd(OAc)_3{\cdot}5.1\ H_2O$, 3:30:67 *v*/*v*/v $H_2O$/MeOH/$CHCl_3$.

Calcd. 1134.8 Da.; Obsd. 1134.8 Da.; $[M + Na]^+$ Calcd. 1156.8 Da.; Obsd. 1156.8 Da.; $[M + 2Na]^+$ Calcd. 1178.7 Da.; Obsd. 1178.8 Da. MALDI-TOF (negative mode): *m*/*z* $[M - H]^-$ Calcd. 1132.5 Da.; Obsd. 1132.6 Da.

### 2.7. Gd(III)DOTA-DSPE (1)

To a solution of **5** (0.50 g, 0.44 mmol) in 9 mL $CHCl_3$ a solution of $Gd(III)(OAc)_3{\cdot}5.1\ H_2O$ (0.18 g, 0.42 mmol, 0.95 equivalents) in 10:1 *v*/*v* MeOH/$H_2O$ (5 mL) was added. Subsequently, the pH was adjusted to 7 using pyridine, and the solution was stirred overnight at room temperature. The formation of the Gd(III) complex was monitored employing analytical RP-HPLC. Since the reaction was performed with a small excess of DOTA-DSPE, the HPLC elution profile showed a large single peak for the Gd(III)DOTA-DSPE and a small single peak for the DOTA-DSPE. The solution was concentrated under reduced pressure and co-evaporated with 1:1 *v*/*v* MeOH/toluene (2 × 10 mL) and $CHCl_3$ (2 × 10 mL) to yield Gd(III) complex **1** (0.52 g, 91%) as a yellowish solid. FT-IR (ATR): *v* ($cm^{-1}$) 3253, 2922, 2852, 1735, 1595, 1465, 1405, 1319, 1201, 1085 and 1064. MALDI-TOF (negative mode): *m*/*z* $[C_{57}H_{105}N_5O_{15}P_1Gd_1 - H]^-$ Calcd. 1287.7 Da.; Obsd. 1287.7 Da.

### 2.8. Liposome preparation

The liposomes were prepared using 1,2-Distearoyl-*sn*-glycero-3-phosphocholine (DSPC), Gd(III)DOTA-DSPE, 1,2-distearoyl-*sn*-Glycero-3-phosphoethanolamine-*N*-[methoxy(polyethylene glycol)-2000] (PEG2000-DSPE) and cholesterol (Chol) at a molar ratio of 1.10/0.75/0.15/1. Liposomes were prepared by lipid film hydration followed by extrusion [12]. A mixture of the appropriate amounts of phospholipids and cholesterol (typically a total amount of 50 μmol) was dissolved in 4:1 *v*/*v* $CHCl_3$/MeOH (10 mL) in a 250 mL round-bottomed flask. This solution was evaporated to dryness using rotation evaporation at 20 mbar and 30 °C. The lipid film was subsequently put under a nitrogen flow overnight to remove traces of organic solvents. Subsequently, the film was heated to 65 °C and hydrated with HEPES buffered saline (HBS) (20 mM HEPES, 135 mM NaCl, pH 7.4) at 65 °C for 10 min. The resulting lipid dispersion was extruded (Lipofast Extruder, Avestin, Ottawa, Ontario) at 65 °C sequentially two times through polycarbonate membrane filters (Whatman, Maidstone, UK) with a pore diameter of 400 nm (typical extrusion pressure: 10–20 bar), 4 times through filters with a pore diameter of 200 nm (20–35 bar) and 6 times through filters with a pore diameter of 100 nm (40–55 bar).

### 2.9. Liposome characterization

Phospholipid concentrations of the liposomal dispersions were determined using two techniques. The first method was a phosphate determination according to Rouser [15] after destruction with perchloric acid at 180 °C. The second method made use of inductively coupled plasma mass spectrometry (ICP-MS, DRCII, Perkin–Elmer, Philips Research Materials Analysis, Eindhoven, Netherlands). Destruction of the samples was performed with nitric acid and perchloric acid at 180 °C. In order to determine the longitudinal relaxivities, Gd(III) concentrations were determined using ICP-MS as well.

### 2.10. DLS and zeta potential measurements

The size and size distribution of the liposomes were determined using dynamic light scattering (DLS) at room temperature on a Malvern Zetasizer Nano S apparatus (Malvern, UK) equipped with

a 633 nm laser. Since the liposomes exhibited a relatively narrow size distribution, a cumulant fit was used for data analysis (Dispersion Technology Software v5.00, Malvern Instruments). The zeta potential of the liposome suspension was determined with the microelectrophoretic method using the Malvern Zetasizer Nano ZS apparatus. Measurements were performed at 20 °C in HBS with 20 mM HEPES, 135 mM NaCl at pH 7.4. Each zeta potential was an average from 1000 measurements.

### 2.11. Cryo-TEM

Cryogenic transmission electron microscopy was used to investigate the size, the size distribution and the morphology of the liposomes. The sample vitrification procedure was carried out using an automated vitrification robot (FEI Vitrobot Mark III). TEM grids, R2/2 Quantifoil Jena grids, were purchased from Aurion (Wageningen, Netherlands). The Quantifoil grids were surface plasma treated using a Cressington 208 carbon coater operating at 5 mA for 40 s prior to the vitrification procedure. Imaging was performed on a FEI Tecnai 20, type Sphera TEM instrument equipped with a LaB6 filament operating at 200 kV. Images were recorded with a bottom-mounted 1kx1k Gatan CCD camera. A Gatan cryoholder operating at −170 °C was used for the cryo-TEM measurements.

### 2.12. Transmetallation

Transmetallation was investigated using the assay developed by Laurent et al. [16]. The MRI contrast agent was dispersed in a phosphate buffer of pH 7 at a Gd(III) concentration of 2.5 mM. This dispersion was kept at 37 °C and at $t = 0$ $ZnCl_2$ was added (Zn(II) concentration: 2.5 mM). Subsequently, the evolution of the longitudinal relaxation rate ($R_1 = 1/T_1$) was monitored using a Bruker Minispec mq60. An inversion recovery sequence with four averages was used. The duration of the 180° pulse was 4.4 ms and of the 90° pulse was 2.2 ms. Ten different inversion times ranging in an exponential fashion from 5 ms to at least 5 times the $T_1$ of the solution were used. The relaxation delay was also set to at least 5 times the $T_1$ of the solution. Transmetallation of Gd(III) by Zn(II) ion leads to the formation of $GdPO_4$, which precipitates in phosphate buffer. $GdPO_4$ does not contribute to $R_1$, and therefore a decrease in $R_1$ is observed proportional to the degree of transmetallation.

### 2.13. $^{17}O$-transverse relaxation rate measurements

$^{17}O$ measurements were performed at 14 T on a Bruker Avance 600 spectrometer. Experimental settings were: spectral width 10 kHz, 90° pulse, acquisition time 10 ms, 128 scans and no sample spinning. The field-frequency lock was carried out on the signal of $CD_3CN$ contained in a capillary coaxially inserted in the 5 mm tube containing the sample. To enhance the detection sensitivity the solutions were enriched in $^{17}O$ isotope (to 2.5%) by adding $^{17}O$ enriched water (10.4% $H_2{}^{17}O$, Yeda R&D Co., Rehovot, Israel). The value of the observed $^{17}O$-transverse relaxation rate was obtained by measuring the linewidth at half height ($\Delta\nu_{12}$) of the water $^{17}O$ signal ($R_2^{obs} = \pi\Delta\nu_{1/2}$). The water exchange correlation time ($\tau_m$) was estimated by analyzing the data according to the Swift and Connick theory [17].

### 2.14. NMRD

z$^1$H NMRD profiles were measured on a Stelar Spinmaster FFC-2000 fast-field cycling relaxometer (Mede, Italy) in a magnetic field range from $2.4 \times 10^{-4}$ to 1.6 T (corresponding to 0.01–70 MHz of proton Larmor frequencies). The $T_1$ relaxation times were acquired by the standard inversion recovery method with typical 90° pulse width of 3.5 μs, using 16 experiments of 4 scans each. The T1 reproducibility was within 5%. The temperature was controlled with a Stelar VTC-91 airflow heater equipped with a calibrated copper constantan thermocouple (precision of 0.1 °C). Measurements were performed at 25 °C (room temperature), 37 °C (physiological temperature), and 60 °C (at a temperature expected to be above the phase-transition temperature of the liposomes). The longitudinal relaxivity $r_1$ was calculated according to Eq. 1 taking into account the diamagnetic contributions of HBS. The NMRD profiles were analyzed according to the Solomon–Bloembergen–Morgan equations modified according to the Lipari–Szabo model free approach [18]. In line with the previous reports [19,18], the water exchange correlation time ($\tau_m$), the number of coordinating water molecules ($q$), the water proton - paramagnetic center distance ($r$), the distance of closest approach ($a$) and the diffusional coefficient ($D$) were kept constant at $\tau_m = 250$ ns, $q = 1$, $r = 3.1$ Å, $a = 3.8$ Å and $D = 2.2 \times 10^{-5}$ cm$^2$ s$^{-1}$ at 25 °C. The global and local rotational correlation times (global and local $\tau_r$), the correlation time for electronic relaxation ($\tau_v$), the order parameter ($S^2$) and the square of the transient of the zero field splitting of the electronic spin states ($\Delta^2$) were allowed to vary.

## 3. Results and discussion

### 3.1. Synthesis of Gd(III)DOTA-DSPE

The strategy for the synthesis of Gd(III)DOTA-DSPE(**1**) is shown in Fig. 1. The synthesis started with the conjugation of *tert*-butyl ester-protected DOTA-based building block **3** to the primary amine of DSPE (**2**). The activation of **3** with HSTU in the presence of DiPEA as a base was performed *in situ* in DMF. To the solution of the activated ester, a solution of DSPE (**2**) in $CHCl_3$ was added. Subsequently, the reaction mixture was heated for 2 h at 45 °C followed by overnight incubation at room temperature. After extraction and precipitation, intermediate **4** was obtained. Structural characterization was performed with $^1$H NMR, RP-HPLC and MALDI-TOF. In the MALDI-TOF spectrum of **4**, the $[M+H]^+$ ion was registered at 1302.8 Da as the most abundant molecular species. The *tert*-butyl esters of **4** were removed with TFA. The quantitative removal of the *tert*-butyl ester moieties was confirmed by the disappearance of their $-CH_3$ signals from the $^1$H NMR spectrum. The reaction of DOTA-DSPE (**5**) with $Gd(OAc)_3$ was performed in 3:30:67 *v*/*v*/*v* $H_2O$/MeOH/$CHCl_3$ with pyridine as a base. In order to prevent the presence of free Gd(III), the complexation reaction was carried out with 1.1 equivalents of **5**. The obtained Gd(III)DOTA-DSPE was characterized by RP-HPLC, FT-IR and MALDI-TOF. As evidenced from the RP-HPLC elution profiles and the MALDI-TOF spectrum of the Gd(III)DOTA-based lipid, a small amount of Gd(III)-free DOTA-DSPE (**5**) (less than 3%) was present (Fig. 2).

### 3.2. Characterization of the liposomes

Gd(III)DOTA-DSPE was incorporated in liposomes containing DSPC/Gd(III)DOTA-DSPE/PEG2000-DSPE/Chol at a molar ratio of 1.10/0.75/0.15/1.00. The liposomes were prepared by lipid film hydration followed by extrusion. The yield of lipids after extrusion (sequentially two times through 400 nm, four times through 200 nm, and eight times through 100 nm filters) was typically 50% as determined with the phosphate determination according to Rouser [15] and ICP-MS. After extrusion through the 200 nm filters, the yield was in the range of 75%. The maximum pressure required to extrude the liposomal dispersion through the 100 and 200 nm filters was 55 and 35 bar, respectively.

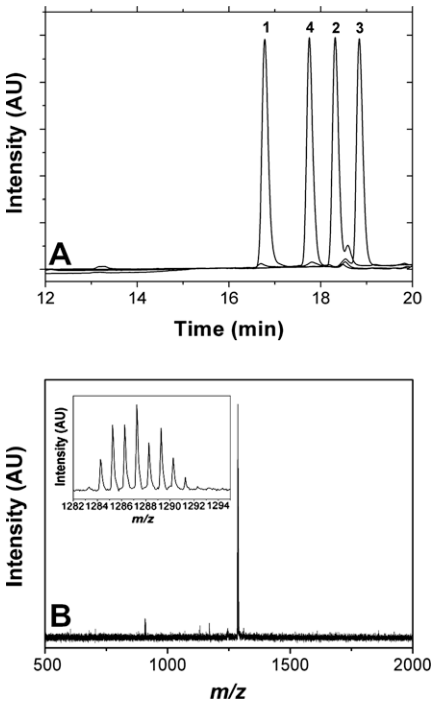


**Fig. 2.** (A) RP-HPLC elution profiles of phospholipids: Gd(III)DOTA-DSPE (1), DSPE (2), Tris-*t*-butyl-DOTA-DSPE (3), DOTA-DSPE (4). (B) MALDI-TOF spectrum of Gd(III)DOTA-DSPE (1), located around $m/z = 1287$. The small peak at $m/z = 900$ represents the 3% of DOTA-DSPE. The inset shows the characteristic isotopic pattern of Gd(III).

### 3.3. DLS

The mean average hydrodynamic diameter of the liposomes was 125 nm with a polydispersity index (PDI) between 0.05 and 0.1. The observed PDI is indicative for liposomes with a narrow size distribution [20,21]. The mean average diameter of liposomes stored at a temperature of 4 °C was studied over a time course of 8 weeks. The size and polydispersity index of the liposomes remained constant. This demonstrates that the steric stabilization of the liposomes by PEG2000-DSPE and cholesterol was effective, resulting in a shelf lifetime of at least 8 weeks. The hydrophilic PEG coating is also known to reduce the interaction of liposomes with molecular and biological components, thereby increasing the *in vivo* circulation time [7,3]. Cholesterol prevents demixing of the lipids and reduces the PEG chain–chain interactions, giving rise to increased steric stabilization and prolonged *in vivo* circulation times of the liposomes. Liposome formulations with long *in vivo* circulation times typically contain over 30% cholesterol and typically less than 7% PEG [3]. It has to be noted that both non-specific and specific uptake of contrast agents *in vivo* increase with increasing circulation times. The course of the target to background ratio as a function of circulation time depends on the properties of the contrast agent and the target, hence long circulation times might not always be advantageous.

### 3.4. Zeta potential

The zeta potential of the liposome formulation was −1.9 mV, i.e., close to neutral. This can be explained by the incorporation of PEG2000-DSPE [22]. The PEG coating is very hydrophilic and therefore highly hydrated, which shields the surface charge of the phospholipids from the bulk water, thereby largely reducing the zeta potential of the particles [23]. Gref et al. showed that a large negative zeta potential led to a significant increase in the non-specific uptake of nanospheres by monocytes *in vitro* [23]. Cationic particles are also readily internalized non-specifically through proteoglycan receptors [24] and, for that reason, are widely employed as non-specific transfection agents. As the liposomes in the present study have almost neutral zeta potential, we expect little electrostatic interactions between the liposomes and anionic cellular membranes and therefore limited non-specific uptake. This is a beneficial property when using the contrast agent for future studies on targeted imaging or targeted image-guided drug delivery.

### 3.5. Cryo-TEM

Cryo-TEM has the unsurpassed ability to visualize individual lipid-based nanoparticles. The vitrification procedure assures that the individual particles can be studied in their natural hydrated state. Fig. 3 shows that the liposome formulation and preparation method resulted in the formation of spherical bilayered vesicles. The morphology of the liposomes was very similar to the morphology of the liposomes reported in the previous work [3]. The majority of the particles consisted of unilamellar liposomes, and no significant aggregation of the liposomes was observed. This confirmed the DLS finding that the liposomes were sufficiently sterically stabilized by the PEG coating and the action of cholesterol to prevent fusion and aggregation after preparation. Inherent to cryo-TEM, only a small fraction of the particles present in a liposome preparation was investigated. As a result, incidental observations in the cryo-TEM images cannot easily be extrapolated to a general finding. Therefore, we investigated at least four independently prepared preparations of the liposomes and several grids per preparation. This led to the finding that besides unilamellar liposomes, multilamellar vesicles (<10%) and disc-shaped micelles (<10%) were present in the liposomal dispersions as well (see arrow and insets in Fig. 3). Due to limited water exchange across the liposomal membranes, the inner leaflet of the lipidic bilayer as well as the inner vesicles in multilamellar particles (illustrated with an arrow in Fig. 3) contribute less to the relaxivity than the outer leaflet [20]. However, some percentage of multilamellar vesicles is considered unavoidable. The *in vivo* behavior of the multi-

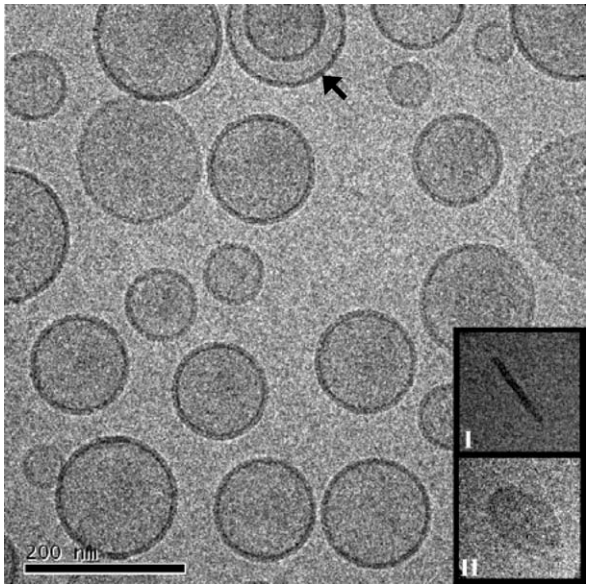


**Fig. 3.** Cryo-TEM image of Gd(III)DOTA-DSPE-based liposomes. The arrow indicates a multilamellar vesicle and the insets depict disc-shaped micelles oriented edge on (I) and face on (II).

lamellar vesicles is not expected to be different from that of unilamellar liposomes as the size is in the same range and the shape, surface coating and zeta potential are identical. The insets in Fig. 3 depict disc-shaped micelles as observed with cryo-TEM. Inset I shows a disc that was oriented edge on and therefore clearly visible. Discs oriented face on are more difficult to detect as the electrons only pass through a single bilayer of lipids, resulting in minimal contrast between the disc and the vitrified ice. However, we were able to visualize these discs as well, as exemplified in inset II.

Johnsson et al. suggest that in disc-like micelles the components are partially segregated. More PEG-lipid is present at the rim to prevent the interaction of the hydrophobic domains with the bulk water, thereby stabilizing the discs, and less PEG-lipid is present in the flat domain of the disc [25]. This model might provide a reasonable description of the discs observed in this study. The composition of the discs is therefore expected to be very similar to the overall composition of the lipid mixture. Moreover, although the presence of discs is undesired, the number of discs is low and hence possible differences in compositions of the discs are not very likely to influence the properties of the remaining liposomes.

Disc-shaped micelles do have a different shape and size than the liposomes, and therefore might behave differently *in vivo* with respect to circulation times and targeting efficiency. Hence, the formation of these structures should be avoided as much as possible. However, several cryo-TEM studies showed that obtaining a single type of aggregate structure, e.g., disc-shaped micelles or liposomes, is essentially impossible to achieve. For example, Glogard et al. prepared disc-shaped micelles containing Gd(III)HHD-DO3A. Besides the desired disc-shaped micelles, they observed globular micelles and liposomes as well [26]. Furthermore, Lokling et al. presented pH sensitive paramagnetic liposomes bearing Gd(III)DTPA-BMA. Apart from the desired unilamellar liposomes, their cryo-TEM images also showed other structures next to liposomes, although these were not explicitly discussed [27].

Despite the fact that cryo-TEM only allowed for the investigation of a small fraction of the nanoparticles and that the interpretation of the images is not always trivial, our studies underscored the importance of cryo-TEM for the characterization of lipid-based nanoparticles. Cryo-TEM is often the only method to evaluate the exact morphology of nanoparticles and therefore an essential tool when studying lipid-based colloidal systems.

### 3.6. Relaxivity

Fig. 4A shows the NMRD curves of the liposomal suspension at 25, 37 and 60 °C. At 25 °C and 1.41 T, close to a typical clinical imaging field strength, the $T_1$-relaxivity per Gd(III) was 11.8 $mM^{-1}$ $s^{-1}$. This is significantly higher in comparison with the $T_1$-relaxivity of Gd(III)DOTA ($r_1 \sim 4$ $mM^{-1}$ $s^{-1}$). The higher ionic $T_1$-relaxivity of the amphiphilic Gd(III) chelate (**1**) incorporated in the liposome is believed to primarily originate from the increased rotational correlation time [12]. The peaks in the NMRD profiles around 30 MHz are characteristic for macromolecular complexes [28], indicating that the higher relaxivity of the Gd(III)DOTA-DSPE compared to Gd(III)DOTA indeed originates from an increase in rotational correlation time. It should be noted here that the relaxivities reported are the average ionic relaxivities of the Gd(III) ions in the inner and outer leaflets of the lipid bilayer. The relaxivity per liposome is obviously much higher as one liposome typically contains 40,000 Gd(III) ions. This number was calculated on the basis of a spherical, unilamellar liposome with a diameter of 125 nm and a lipid surface area of 0.6 $nm^2$ [29].

Although the ionic relaxivities of Gd(III)DTPA and Gd(III)DOTA are both around 4 $mM^{-1}$ $s^{-1}$, the ionic relaxivity of the Gd(III)DOTA-DSPE incorporated in liposomes was significantly higher than

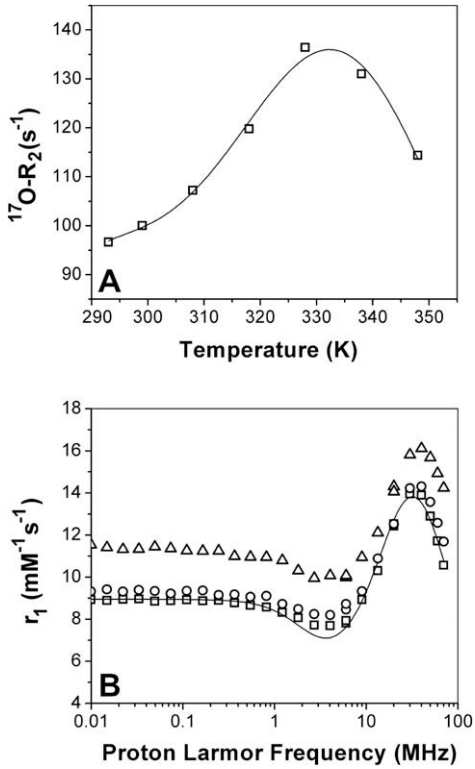


**Fig. 4.** (A) The temperature dependence of the transverse relaxation rate for $^{17}$O-water in the liposomal dispersion. (B) NMRD-profiles of Gd(III)DOTA-DSPE containing liposomal dispersions, as measured at temperatures of 25 °C (□), 37 °C (○) and 60 °C (Δ). The line represents the best fit of the experimental data obtained at 25 °C according to the Solomon–Bloembergen–Morgan equations modified according to Lipari–Szabo model free approach.

that of Gd(III)DTPA-BSA in liposomes ($r_1 \sim 7.0$ $mM^{-1}$ $s^{-1}$ at 25 °C and 1.41 T) reported in our previous studies [12,3]. At 37 °C and 1.41 T, Gd(III)DOTA-DSPE and Gd(III)DTPA-BSA exhibited relaxivities of 12.8 $mM^{-1}$ $s^{-1}$ and 7.5 $mM^{-1}$ $s^{-1}$, respectively. The analysis of the temperature dependence of the transverse relaxation rate for $^{17}$O-water in the Gd(III)DOTA-DSPE liposome suspension allowed the estimation of $\tau_m$ of the metal coordinated water molecule in the incorporated complex (Fig. 4A). The $\tau_m$ value was estimated to amount to 250 ns at 25 °C. This is significantly shorter than the $\tau_m$ that was previously reported for liposome-incorporated Gd(III)DTPA-BSA (1200 ns at 25 °C [3]). This pronounced difference in $\tau_m$ for Gd(III)DTPA-BSA and Gd(III)DOTA-DSPE might be explained by the difference in their overall structure. In the case of Gd(III)DTPA-BSA, the polar head group consists of the Gd(III)DTPA complex. As a consequence, the Gd(III)DTPA is positioned at the interface between the liposomal membrane and the bulk water. For Gd(III)DOTA-DSPE, the Gd(III)DOTA complex is conjugated to the primary amine of DSPE (Fig. 1). In this case, the phosphate group is presumably positioned at the interface of the lipid bilayer and the bulk water. Consequently, the Gd(III)DOTA complex extends from the membrane, resulting in better access for water molecules to the paramagnetic complex as compared to Gd(III)DTPA-BSA, which may thus explain the higher relaxivity. This finding agrees well with that of Winter et al., who also reported that the relaxivity of Gd(III)DOTA attached to PE was significantly higher than the relaxivity of Gd(III)DTPA-BOA when incorporated in their emulsions [30,31]. These authors also demonstrated that a longer spacer results in a higher relaxivity [30]. With increasing length of the spacer the accessibility for water molecules might increase, while at the same time the rotational correlation time of the Gd(III) chelate decreases due to increased flexibility. The latter effect will

result in lowering of the relaxivity. The optimal length of the spacer in our novel paramagnetic lipid species remains to be determined.

Another issue that might partly explain the high relaxivity of Gd(III)DOTA-DSPE is the presence of disc-shaped micelles in the suspension (Fig. 3). As the inner leaflet of the liposomal membranes hardly contributes to the overall relaxivity (due to limited water exchange), the presence of discs, in which all paramagnetic lipids face the bulk water, increases the ionic $T_1$-relaxivity. However, the fraction of discs in this formulation was relatively low (<10%) and, hence, the large difference in relaxivity between the Gd(III)DOTA-DSPE and Gd(III)DTPA-BSA cannot be attributed to this phenomenon alone.

The NMRD measurements showed that an increase in temperature led to an increase in relaxivity (Fig. 4B). This is probably due to the increased water exchange across the liposomal membrane at higher temperature, resulting in a higher contribution of Gd(III)DOTA-DSPE in the inner leaflet to the overall $T_1$-relaxivity [12]. Fitting of the NMRD data was only successful for the curve measured at 25 °C. We hypothesize that this has to do with increasing water exchange over the liposomal membrane with increasing temperature. Consequently, the contribution of the Gd(III) complexes in the inner leaflet to the overall relaxivity increases with temperature. The present fitting model does not account for this phenomenon, and therefore the fitting of the NMRD curves at 37 °C and 60 °C failed to converge. The fit of the NMRD curve obtained at 25 °C is shown in Fig. 4B. The global $\tau_r$ was estimated to be 2.6 ns, while $\tau_v$ was 37 ps. The global $\tau_r$ and $\tau_v$ are similar for the Gd(III)DTPA-BSA liposomes [3], indeed suggesting that the increased relaxivity of the Gd(III)DOTA-DSPE liposomes is mainly due to the decreased $\tau_m$.

### 3.7. Transmetallation

Several studies have shown that endogenous cations can replace the Gd(III) ion in Gd(III) complexes both *in vitro* [16,32] and *in vivo* [33–35], a process known as transmetallation. Transmetallation induces the release of Gd(III) ions from the chelate. Free Gd(III) ions can block calcium channels [33], and can be deposited as insoluble salts in bone, liver and spleen [35]. Another issue concerning transmetallation of Gd(III) complexes by endogenous ions is that depletion of these endogenous ions by the chelate may occur [34]. The linear, open-chain Gd(III)-chelates such as Gd(III)DTPA and Gd(III)DTPA-BMA were shown to be very sensitive for transmetallation [16,32]. Administration of Gd(III)DTPA-BMA to patients with renal failure has recently been related to nephrogenic systemic fibrosis [36]. Although the exact cause of this severe disorder has not been determined yet, it is of great importance to find and implement alternatives for the linear DTPA and DTPA-derived Gd(III)-chelates. The macrocyclic chelates such as Gd(III)DOTA and Gd(III)HP-DO3A have been demonstrated to be very stable [16,32]. Therefore, we decided to conjugate the macrocyclic DOTA chelate to DSPE. We studied the transmetallation of Gd(III)DOTA-DSPE and compared it to transmetallation of Gd(III)DTPA-BSA, using the assay according to Laurent et al. [16]. Gd(III)DTPA-BSA served as a reference compound, since it has been previously used in a number of our lipid-based MRI contrast agents [37,12,7,3,11].

In this transmetallation assay, Zn(II) is used as the ion competing with Gd(III). The binding affinity of Zn(II) for organic ligands is only about 4 times lower than that of Gd(III) [38], and the blood concentration of the Zn(II) ion is 55–125 μM. Therefore, this ion is expected to bring about the most significant transmetallation *in vivo*. Other endogenous ions likely to transmetallate Gd(III)-chelates are Cu(II) and Ca(II). However, Ca(II) has a binding affinity for organic ligands about ten times lower than that of Gd(III) and Cu(II) concentrations in blood are very low (1–10 μM) [39].

In Fig. 5A the results of the transmetallation assay are presented, showing the normalized relaxation rate ($R_1(t)/R_1(t=0)$) as a function of time after adding $Zn(II)Cl_2$. To validate our experimental set up, Gd(III)-HPDO3A and Gd(III)DTPA were included as controls. For Gd(III)-HPDO3A, the normalized relaxation rate remained unchanged after the addition of $Zn(II)Cl_2$, indicating that no transmetallation took place, while for Gd(III)DTPA a significant decrease was observed. These findings are in agreement with the observations reported by Laurent et al. [16]. For the Gd(III)DOTA-DSPE liposomes, the normalized relaxation rate showed an essentially instantaneous drop of approximately 25–30% upon the addition of $Zn(II)Cl_2$, after which the relaxation rate remained constant over time. A titration with EDTA, which complexes free Zn(II) ions, resulted in a complete recovery of $R_1(t)/R_{1,t=0}$ to its starting value of 1.0 (Fig. 5B), thereby demonstrating that no transmetallation between Zn(II) and Gd(III) had occurred. Binder et al. observed that Zn(II) strongly interacts with the negatively charged phospholipid groups in POPC vesicles. This led to partial dehydration of the lipids, which effectively rendered the membrane surface more hydrophobic [40]. This effect might decrease the accessibility of the Gd(III)DOTA-ligands for water molecules, thereby influencing the relaxivity of the liposomes. A similar observation was made for emulsions of Gd(III)DOTA-conjugated nanoparticles [30]. For Gd(III)DTPA-BSA, the normalized relaxation rate showed a fast decrease upon the addition of Zn(II) ions (Fig. 5A), indicating that rapid transmetallation occurred. In this case, the subsequent addition of EDTA did not lead to a change in relaxation rate (data not shown). The high stability of Gd(III)DOTA-DSPE-based liposomes against transmetallation with Zn(II) is in good agreement with the literature studies on emulsions of Gd(III)DOTA-functionalized nanoparticles [30]. The strongly increased stability of Gd(III)DOTA-DSPE in comparison with Gd(III)DTPA-BSA represents an important improvement of the liposomal MRI contrast agent.

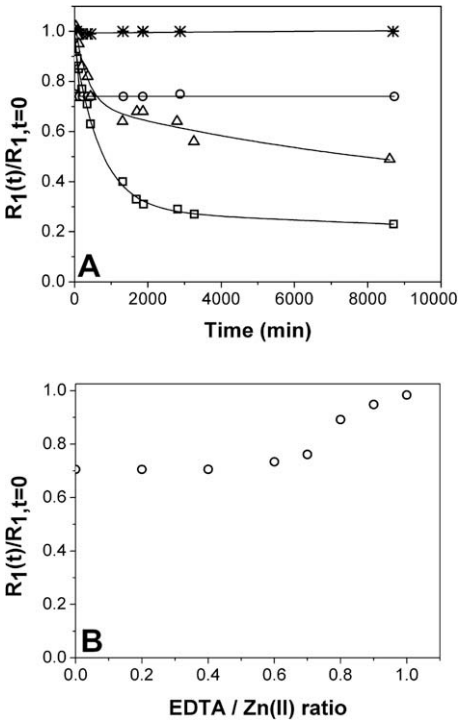


**Fig. 5.** Results of the transmetallation assay. (A) $R_1(t)/R_{1,t=0}$ as a function of time after adding the Zn(II) ions at $t = 0$, as measured for of Gd(III)DOTA-DSPE liposomes (○), Gd(III)-HPDO3A (*), Gd(III)DTPA-BSA liposomes (□) and Gd(III)DTPA (Δ). The lines serve as guide to the eye. (B) Evolution of $R_1(t)/R_{1,t=0}$ of a Gd(III)DOTA-DSPE liposomal suspension as a function of the amount of EDTA relative to the amount of Zn(II) added to the transmetallation buffer.

## 4. Conclusion

We described the preparation and *in vitro* characterization of paramagnetic liposomes containing Gd(III)DOTA-DSPE. The liposomes were shown to have a significantly increased longitudinal relaxivity compared to Gd(III)DTPA-BSA-based liposomes. This is crucial for the detection of low concentration molecular markers in MRI-based molecular imaging studies. Gd(III)DOTA-DSPE exhibits no significant transmetallation upon incubation with Zn(II), which significantly improves the biocompatibility of the contrast agent. Furthermore, the zeta potential of the liposome formulation is almost neutral, which is expected to result in low non-specific cellular uptake.

The versatility of the liposomal preparation lies in the fact that the particles can easily be made multimodal, for example by incorporating fluorescent lipids, and a wide variety of targeting ligands can be conjugated to the distal ends of the PEG chains. Furthermore, drugs can readily be encapsulated in the lumen or the membrane of the liposomes. The presented liposome preparation can thus serve as a versatile and well characterized platform for molecular imaging and targeted drug delivery studies.

## Acknowledgments

The authors thank Willem Mulder for useful discussions. This study was funded in part by the Integrated EU Project MEDITRANS (FP6-2004-NMP-NI-4/IP 026668-2), the BSIK program entitled Molecular Imaging of Ischemic Heart Disease (project number BSIK03033) and by the EC—FP6-project DiMI, LSHB-CT-2005-512146. This study was performed in the framework of the European Cooperation in the field of Scientific and Technical Research (COST) D38 Action Metal-Based Systems for Molecular Imaging Applications.

## References

[1] R. Weissleder, U. Mahmood, Molecular imaging, Radiology 219 (2) (2001) 316–333.
[2] G.A. Koning, G.C. Krijger, Targeted multifunctional lipid-based nanocarriers for image-guided drug delivery, Anticancer Agents Med. Chem. 7 (4) (2007) 425–440.
[3] G.J. Strijkers, W.J. Mulder, R.B. van Heeswijk, P.M. Frederik, P. Bomans, P.C. Magusin, K. Nicolay, Relaxivity of liposomal paramagnetic MRI contrast agents, Magma 18 (4) (2005) 186–192.
[4] D.C. Drummond, O. Meyer, K. Hong, D.B. Kirpotin, D. Papahadjopoulos, Optimizing liposomes for delivery of chemotherapeutic agents to solid tumors, Pharmacol. Rev. 51 (4) (1999) 691–743.
[5] S.M. Moghimi, A.C. Hunter, J.C. Murray, Long-circulating and target-specific nanoparticles: theory to practice, Pharmacol. Rev. 53 (2) (2001) 283–318.
[6] N. Kamaly, T. Kalber, A. Ahmad, M.H. Oliver, P.W. So, A.H. Herlihy, J.D. Bell, M.R. Jorgensen, A.D. Miller, Bimodal paramagnetic and fluorescent liposomes for cellular and tumor magnetic resonance imaging, Bioconjug. Chem. 19 (1) (2008) 118–129.
[7] W.J. Mulder, G.J. Strijkers, J.W. Habets, E.J. Bleeker, D.W. van der Schaft, G. Storm, G.A. Koning, A.W. Griffioen, K. Nicolay, MR molecular imaging and fluorescence microscopy for identification of activated tumor endothelium using a bimodal lipidic nanoparticle, FASEB J. 19 (14) (2005) 2008–2010.
[8] V. Amirbekian, M.J. Lipinski, K.C. Briley-Saebo, S. Amirbekian, J.G. Aguinaldo, D.B. Weinreb, E. Vucic, J.C. Frias, F. Hyafil, V. Mani, E.A. Fisher, Z.A. Fayad, Detecting and assessing macrophages in vivo to evaluate atherosclerosis noninvasively using molecular MRI, Proc. Natl. Acad. Sci. USA 104 (3) (2007) 961–966.
[9] W.J. Mulder, G.J. Strijkers, K.C. Briley-Saboe, J.C. Frias, J.G. Aguinaldo, E. Vucic, V. Amirbekian, C. Tang, P.T. Chin, K. Nicolay, Z.A. Fayad, Molecular imaging of macrophages in atherosclerotic plaques using bimodal PEG-micelles, Magn. Reson. Med. 58 (6) (2007) 1164–1170.
[10] D.A. Sipkins, K. Gijbels, F.D. Tropper, M. Bednarski, K.C. Li, L. Steinman, ICAM-1 expression in autoimmune encephalitis visualized using magnetic resonance imaging, J. Neuroimmunol. 104 (1) (2000) 1–9.
[11] G.A. van Tilborg, W.J. Mulder, N. Deckers, G. Storm, C.P. Reutelingsperger, G.J. Strijkers, K. Nicolay, Annexin A5-functionalized bimodal lipid-based contrast agents for the detection of apoptosis, Bioconjug. Chem. 17 (3) (2006) 741–749.
[12] W.J. Mulder, G.J. Strijkers, A.W. Griffioen, L. van Bloois, G. Molema, G. Storm, G.A. Koning, K. Nicolay, A liposomal system for contrast-enhanced magnetic resonance imaging of molecular targets, Bioconjug. Chem. 15 (4) (2004) 799–806.
[13] A. Dadabhoy, F.S. Sammes, P.G. Long, wavelength sensitizers for europium(iii) luminescence based on acridone derivatives, J. Chem. Soc. Perkin Trans. 2 (2) (2002) 348–357.
[14] L.M. De León-Rodríguez, Z. Kovacs, The synthesis and chelation chemistry of DOTA–peptide conjugates, Bioconjug. Chem. 19 (2) (2008) 391–402.
[15] G. Rouser, Two dimensional thin layer chromatographic separation of polar lipids and determination of phospholipids by phosphorus analysis of spots, Lipids (1970).
[16] S. Laurent, L.V. Elst, F. Copoix, R.N. Muller, Stability of MRI paramagnetic contrast media: a proton relaxometric protocol for transmetallation assessment, Invest. Radiol. 36 (2) (2001) 115–122.
[17] T.J. Swift, R.E. Connick, NMR-relaxation mechanisms of O17 in aqueous solutions of paramagnetic cations and the lifetime of water molecules in the first coordination sphere, J. Chem. Phys. 37 (1962) 307.
[18] J. Rudovski, M. Botta, P. Hermann, K.I. Hardcastle, I. Lukes, S. Aime, Bioconjug. Chem. 17 (4) (2006) 975–987.
[19] S. Aime, I.M. Botta, F. Fedeli, E. Gianolio, E. Terreno, P. Anelli, High-Relaxivity contrast agents for magnetic resonance imaging based on multisite interactions between a beta-cyclodextrin oligomer and suitably functionalized GdIII chelates, Chemistry 7 (24) (2001) 5261–5269.
[20] E. Terreno, A. Sanino, C. Carrera, D.D. Castelli, G.B. Giovenzana, A. Lombardi, R. Mazzon, L. Milone, M. Visigalli, S. Aime, Determination of water permeability of paramagnetic liposomes of interest in MRI field, J. Inorg. Biochem. (2008).
[21] S.W. Zielhuis, J.H. Seppenwoolde, V.A. Mateus, C.J. Bakker, G.C. Krijger, G. Storm, B.A. Zonnenberg, A.D. van het Schip, G.A. Koning, J.F. Nijsen, Lanthanide-loaded liposomes for multimodality imaging and therapy, Cancer Biother. Radiopharm. 21 (5) (2006) 520–527.
[22] T.S. Levchenko, R. Rammohan, A.N. Lukyanov, K.R. Whiteman, V.P. Torchilin, Liposome clearance in mice: the effect of a separate and combined presence of surface charge and polymer coating, Int. J. Pharm. 240 (1–2) (2002) 95–102.
[23] R. Gref, G. Miralles, É. Dellacherie, Polyoxyethylene-coated nanospheres: effect of coating on zeta potential and phagocytosis, Polym. Int. 48 (1999) 251–256.
[24] S.R. Popielarski, S.H. Pun, M.E. Davis, A nanoparticle-based model delivery system to guide the rational design of gene delivery to the liver. 1. Synthesis and characterization, Bioconjug. Chem. 16 (5) (2005) 1063–1070.
[25] M. Johnsson, K. Edwards, Liposomes, disks, and spherical micelles: aggregate structure in mixtures of gel phase phosphatidylcholines and poly(ethylene glycol)-phospholipids, Biophys. J. 85 (6) (2003) 3839–3847.
[26] C. Glogard, G. Stensrud, J. Klaveness, Novel high relaxivity colloidal particles based on the specific phase organisation of amphiphilic gadolinium chelates with cholesterol, Int. J. Pharm. 253 (1–2) (2003) 39–48.
[27] K.E. Lokling, R. Skurtveit, A. Bjornerud, S.L. Fossheim, Novel pH-sensitive paramagnetic liposomes with improved MR properties, Magn. Reson. Med. 51 (4) (2004) 688–696.
[28] C. Glogard, G. Stensrud, R. Hovland, S.L. Fossheim, J. Klaveness, Liposomes as carriers of amphiphilic gadolinium chelates: the effect of membrane composition on incorporation efficacy and in vitro relaxivity, Int. J. Pharm. 233 (1–2) (2002) 131–140.
[29] M. Dekker, Phospholipids Handbook, Marcel Dekker Inc., New York, 1993.
[30] P.M. Winter, P. Athey, G. Kiefer, G. Gulyas, K. Frank, R. Fuhrhop, D. Robertson, S.A. Wickline, G.M. Lanza, Improved paramagnetic chelate for molecular imaging with MRI, J. Magn. Magn. Mater. 293 (1) (2005) 540–545.
[31] P.M. Winter, S.D. Caruthers, X. Yu, S.K. Song, J. Chen, B. Miller, J.W. Bulte, J.D. Robertson, P.J. Gaffney, S.A. Wickline, G.M. Lanza, Improved molecular imaging contrast agent for detection of human thrombus, Magn. Reson. Med. 50 (2) (2003) 411–416.
[32] M. Port, J.M. Idee, C. Medina, C. Robic, M. Sabatou, C. Corot, Efficiency, thermodynamic and kinetic stability of marketed gadolinium chelates and their possible clinical consequences: a critical review, Biometals (2008).
[33] B.A. Biagi, J.J. Enyeart, Gadolinium blocks low- and high-threshold calcium currents in pituitary cells, Am. J. Physiol. 259 (3 Pt 1) (1990) C515–C520.
[34] N.R. Puttagunta, W.A. Gibby, G.T. Smith, Human in vivo comparative study of zinc and copper transmetallation after administration of magnetic resonance imaging contrast agents, Invest. Radiol. 31 (12) (1996) 739–742.
[35] S.M. Rocklage, D. Worah, S.H. Kim, Metal ion release from paramagnetic chelates: what is tolerable?, Magn Reson. Med. 22 (2) (1991) 216–221. discussion 229–32.
[36] P. Marckmann, Nephrogenic systemic fibrosis: epidemiology update, Curr. Opin. Nephrol. Hypertens. 17 (3) (2008) 315–319.
[37] W.J. Mulder, R. Koole, R.J. Brandwijk, G. Storm, P.T. Chin, G.J. Strijkers, C. de Mello Donega, K. Nicolay, A.W. Griffioen, Quantum dots with a paramagnetic coating as a bimodal molecular imaging probe, Nano Lett. 6 (1) (2006) 1–6.
[38] M.F. Tweedle, J.J. Hagan, K. Kumar, S. Mantha, C.A. Chang, Reaction of gadolinium chelates with endogenously available ions, Magn. Reson. Imaging 9 (3) (1991) 409–415.
[39] W.P. Cacheris, S.C. Quay, S.M. Rocklage, The relationship between thermodynamics and the toxicity of gadolinium complexes, Magn. Reson. Imaging 8 (4) (1990) 467–481.
[40] H. Binder, K. Arnold, A.S. Ulrich, O. Zschornig, Interaction of $Zn^{2+}$ with phospholipid membranes, Biophys. Chem. 90 (1) (2001) 57–74.